Telomere attrition and genomic instability in xeroderma pigmentosum type-b deficient fibroblasts under oxidative stress

Aloysius Poh Leong Ting, Grace Kah Mun Low, Kalpana Gopalakrishnan, M. Prakash Hande *

Department of Physiology, Yong Loo Lin School of Medicine, National University of Singapore, Singapore

Abstract

Xeroderma pigmentosum B (XPB/ERCC3/p89) is an ATP-dependent $3' \rightarrow 5'$ directed DNA helicase involved in basal RNA transcription and the nucleotide excision repair (NER) pathway. While the role of NER in alleviating oxidative DNA damage has been acknowledged it remains poorly understood. To study the involvement of XPB in repair of oxidative DNA damage, we utilized primary fibroblasts from a patient suffering from XP with Cockayne syndrome and hydrogen peroxide (H_2O_2) to induce oxidative stress. Mutant cells retained higher viability and cell cycle dysfunction after H_2O_2 exposure. Cytokinesis blocked micronucleus assay revealed increased genome instability induced by H_2O_2. Single cell gel electrophoresis (comet) assay showed that the missense mutation caused a reduced repair capacity for oxidative DNA damage. Mutant fibroblasts also displayed decreased population doubling rate, increased telomere attrition rate and early emergence of senescent characteristics under chronic low dose exposure to H_2O_2. Fibroblasts from a heterozygous individual displayed intermediate traits in some assays and normal traits in others, indicating possible copy number dependence. The results show that a deficiency in functional XPB paradoxically renders cells more sensitive to the genotoxic effects of oxidative stress while reducing the cytotoxic effects. These findings have implications in the mechanisms of DNA repair, mutagenesis and carcinogenesis and ageing in normal physiological systems.

Introduction

Damage resulting from exposure to both endogenous and exogenous genotoxic agents can alter DNA and interfere with DNA replication and protein transcription, which ultimately predisposes cancer, and developmental defects [1]. DNA damage may also occur at telomeres, a process which can compromise their integrity. As telomeres are important factors in genome stability and replication competency, damaged telomeres can lead to outcomes such as genomic instability and premature senescence [2–6]. Mammals have evolved to be equipped with DNA repair mechanisms that specifically operate for individual base damages as well as genome repair through recognizing specific DNA helix distortions, one of which is the most versatile nucleotide excision repair (NER) pathway [7].

Reactive oxygen species (ROS) are known to cause oxidative damage to cellular components, as well as a multitude of DNA lesions [8]. Hydrogen peroxide (H_2O_2) is an endogenously produced ROS, generated during oxidative energy metabolism and exposure to exogenous factors such as lead compounds. Similar to UV-induced DNA damage, oxidative DNA damage gives rise to helix distortions that hinder base pairing, transcription and replication. Accumulation of unrepaired oxidative lesions predisposes cancer [1] and shortens telomeres [9], leading to premature senescence and possibly ageing.

Xeroderma pigmentosum (XP) is a rare autosomal recessive congenital DNA repair disorder stemming from defects in the NER. This syndrome manifests as segmental progeria, sunlight hypersensitivity, a 1000-fold increase in risk of cutaneous cancers and a host of other developmental and neurological abnormalities. Defects in the NER can also cause Cockayne's syndrome and trichothiodystrophy [1, 10, 11].

The NER pathway engages a multiplex of proteins in a spatially and temporally specific manner to excise primarily bulky lesions including UV-induced pyrimidine dimers [11]. Though oxidative lesions are mainly resolved by the base excision repair (BER) pathway, the NER

*Correspondence to: M. Prakash HANDE, Ph.D.,
Genome Stability Laboratory, Department of Physiology,
Yong Loo Lin School of Medicine, National University of Singapore,
Block MD9, 2 Medical Drive, Singapore 117597, Singapore.
Tel.: +65-6516-3664
Fax: +65-6778-8161
E-mail: phsmph@nus.edu.sg

pathway has also been implicated in the repair of some of these lesions [1, 12, 13]. This process is however still poorly characterized.

XPB is a $3' \to 5'$ helicase in the NER pathway and a subunit of the RNA polymerase II holoenzyme TFIIH. XPB plays a key role in the NER by unwinding the DNA helix surrounding the lesion and thus allowing access by subsequent factors. Studies have also shown roles for XPB in the incision [14] and excision [15] of lesions and in the recruitment of other NER factors to lesion sites [16]. As a subunit of TFIIH, XPB also plays a role in basal transcription [17]. As such, XPB mutation can give rise to all three NER dysfunction syndromes [18]. XPB is a member of the helicase domain containing family of proteins. Other members of this family including WRN and BLM have been shown to have a role in telomere maintenance [19–22]. Additionally, it has been reported that the NER endonuclease XPF is involved in telomere dynamics in mice overexpressing telomere restriction fragment (TRF)2 [23].

The hitherto poorly defined role of the NER and its helicase XPB in oxidative DNA lesion repair and telomere dynamics in contrast to the known and reported functions of the BER and its helicase WRN in these processes led us to investigate the possible role of the XPB in genome stability and telomere dynamics under oxidative stress.

Materials and methods

Cell culture and H_2O_2 treatment

Our study utilizes primary fibroblasts from individuals heterozygous for dysfunctional XPB as a result of a splice donor mutation in intron 3 (c.471+1G>A) with the second allele being either dysfunctional as well due to a missense mutation (p.F99S) or normal (henceforth designated XPB$^{-/-}$ and XPB$^{+/-}$, respectively) and normal primary fibroblasts [24, 25]. There are clinical differences among XPB patients with the same p.F99S mutation. Primary human diploid fibroblasts from a normal individual (normal GM03651E; female, 25 years; passage 10), an individual suffering from XP complementation group B (XPB$^{-/-}$ GM13026; male, 25 years; passage 10) and the unaffected mother of the XPB patient (XPB$^{+/-}$ GM13027; female, 63 years; and passage 10) were purchased from Coriell Cell Repositories (Camden, NJ, USA), and cultured in minimal essential medium (Gibco, Grand Island, NY, USA) supplemented with 15% foetal bovine serum (FBS; Hyclone, Logan Town, UT, USA), 100 U/ml penicillin/streptomycin, 1% vitamins, and 2% essential and 1% non-essential amino acid. All cells were grown in a humidified 5% CO_2 incubator at 37°C and maintained in a log phase. All other supplements unless otherwise stated were from Gibco. Cells at passages between 13 and 15 were used in the experiments. Exponentially growing cells were exposed to 20 μM, 40 μM, 60 μM, 80 μM and 100 μM of H_2O_2 (Kanto Chemical Co. Inc., Tokyo, Japan) for 2 hrs, following which the medium was replaced with fresh medium for a 22-hr recovery period.

Crystal violet assay

Crystal Violet dye binds electrostatically to nuclear proteins and thus stains DNA. Upon elimination of excess dye and solubilization of the dye, the relative density of adhered cells can be measured, which correlates to live cell number. Following treatment with different doses of H_2O_2, cells were washed gently in PBS (NUMI supplies, Singapore). Crystal Violet solution (0.75% crystal violet in 50% ethanol: distilled water with 1.75% formaldehyde and 0.25% NaCl) was gently added to the wells and incubated at room temperature, then washed in PBS. Thereafter, the wells were air-dried. A total of 1% SDS (NUMI supplies) in PBS was added to lyse the cells and solubilize the dye. Solution absorbance at 595 nm was measured in an ELISA plate reader.

Cell cycle analysis by fluorescence activated cell sorting

Control and treated cells were fixed in 3:1 70% ethanol: PBS, and subsequently stained with propidium iodide (PI, Sigma, St Louis, MO, USA): RNase A (Roche, Indianapolis, IN, USA) solution (2 mg PI and 2 mg RNaseA/ 100 ml 0.1% BSA in 1×PBS). Samples were analysed by flow cytometry at 488 nm excitation λ and 610 nm emission λ. Ten thousand events were collected and the data obtained was analysed using WINMDI software.

Cytokinesis blocked micronucleus analysis

After 2 hrs exposure to H_2O_2, cells were incubated in a fresh medium with 4.0 μg/ml cytochalasin B (Sigma) for 22 hrs. The protocol used is adapted from Hande *et al.* [26, 27]. Cells were subjected to hypotonic swelling in cold 0.075 M potassium chloride (KCl) and processed as previously described [28]. One thousand binucleated cells with/without micronuclei were scored under the Axioplan 2 imaging fluorescent microscope (Carl Zeiss, Oberkochen, Germany) with the appropriate filters.

Chromosome aberration analysis by peptide nucleic acid- fluorescence *in situ* hybridization (PNA-FISH)

Treated cells were allowed to grow in fresh medium for 24 hrs before being arrested at metaphase with 0.1 μg/ml colcemid for chromosome preparation. FISH and analysis were performed as described before [28] using Cy3-labelled PNA-telomeric and FITC-labelled PNA-centromeric probes (Applied Biosystems, Foster City, CA, USA) [29].

Alkaline single cell gel electrophoresis (Comet) assay

Cells were harvested for Comet assay after 2-hr exposure to H_2O_2 and after 22 hr recovery. Cells were resuspended in Hank's balanced salt solution (HBSS; Sigma), mixed with 0.7% low melting point agarose (Conda, Madrid, Spain) and applied on Comet slides (Trevigen, Gaithersburg, MD, USA). Embedded cells were subjected to in lysis (2.5 M NaCl, 0.1 M pH 8 ethylenediaminetetraacetic acid [EDTA], 10 mM Tris base, 1% Triton X) at 4°C for 1 hr. After lysis, the slides were loaded onto a gel electrophoresis tank and immersed alkaline electrophoresis buffer (0.3 M NaOH buffered at pH 13–13.8 with 0.5 M EDTA pH 8.0) for 40 min. to allow DNA denaturation before being run at a constant 25 V/300 mA for 20 min. Following run, samples were neutralized with 0.5 M Tris-HCl pH 7.5 (NUMI supplies) for

15 min., dehydrated in 70% ethanol for 5 min., and then dried at 37°C. DNA was stained using SYBR Green (Trevigen). Analysis of comets was performed with Comet Imager Software (Metasystems, Altlussheim, Germany). Extent of DNA damage was expressed as a measure of the percentage of DNA in the comet tails. One hundred randomly selected cells were examined per sample.

Cellular kinetic studies

Treatment
Cells were seeded in T75 flasks at a density of 2×10^5 cells per flask and subjected to a 30-day long-term chronic treatment. One set of cells was treated with 20 μM H_2O_2 every 48 hrs, with media changed prior to addition of drug; another set of cells was maintained in a 40% O_2 incubator, with media changed every 48 hrs; media for control cells was also changed every 48 hrs.

Morphological analysis
Cells were observed under a light microscope at 40$\times$, 100$\times$ and 200$\times$ magnifications before media changes. Morphology of the cells was photographed using an Olympus C-7070 WZ (Tokyo, Japan) digital camera.

Population doubling (PD) study
Cells were harvested whenever 90% confluency was reached for untreated cells of each cell type, and on the final day of the experiment. This occurred on days 6, 12, 18, and 30. Harvested cells were counted using a haemocytometer. A fresh tissue culture flask was then reseeded with 2×10^5 cells or all cells if cell numbers were less than 2×10^5.

The population doubling number (PDN) was calculated as follows:

$$PDN = \log_2 (N_0 / N_x),$$

where N_0 = number of cells at harvest and N_x = number of cells seeded [30].

A portion of the remaining cells was seeded in 6-well culture plates (NUNC) for senescence-associated β-galactosidase (SA-β-gal) assay and the rest kept for DNA extraction for TRF analysis.

Senescence-associated β-galactosidase (SA-β-Gal) assay
Expression of SA-β-gal was performed with the Senescence β-Galactosidase Staining Kit (Cell Signaling Technology, Denvers, MA, USA) following manufacturer's instructions. Cells were observed under a light microscope at 40$\times$, 100$\times$ and 200$\times$ magnifications, and cell photographs taken with an Olympus C-7070 WZ digital camera.

Telomere restriction fragment length analysis
DNA was extracted from the cells using DNeasy Tissue Kit (Qiagen, Valencia, CA, USA) according to manufacturer's instructions. The telomere lengths of these cells were measured using TeloTAGGG Telomere Length Assay Kit (Roche Applied Science, USA). Two μg of purified DNA was digested with *HinfI* and *RsaI* for 2 hrs at 37°C. DNA fragments were separated by gel electrophoresis in 0.8% agarose gel at 60 V for 3 hrs, transferred *via* over night Southern blot onto a nylon membrane and cross-linked onto the membrane using a UV cross-linker (Stratagene, La Jolla, CA, USA). TRFs were hybridized with telomere-specific digoxigenin (DIG)-labelled probe and incubated with Anti-DIG alkaline phosphatase

and tetramethylbenzidine according to manufacturer's protocol. Chemiluminescence signal was detected using X-ray film and telomere length was analysed using GeneTools software (SYNGENE, Cambridge, UK). Decrease in telomere length was then expressed as a function of PDN to assess the rate of telomere shortening, indicating the effect of drug treatment on telomeres.

Western analysis for XPB and p53 proteins

Cells were seeded, as described above and harvested at 2, 24 and 48 hrs after exposure to H_2O_2. Total cellular protein was extracted by lysing cells in 100–200 μl lysis buffer (10 mM Tris-HCl [pH 7.4], 1% SDS, 1 mM sodium ortho-vanadate in ddH$_2$O). Released DNA was sheared by passing the lysate through a 0.4×12 mm syringe (100 Sterican, B. BRAUN, Melsungen, Germany). Lysed cells were centrifuged at 13.2 rpm, for 6 min. at 4°C, and the supernatants collected. Protein concentrations were determined using the micro BCA Protein Assay kit (Pierce, Rockford, IL, USA). One μl of cell lysate was diluted in 249 μl of dH$_2$O and 250 μL micro BCA working reagent (25 parts solution A: 24 parts solution B: 1 part solution C) and quantified against known concentrations of BSA (1 μg/ml -40 μg/ml). Forty micrograms protein from each sample was loaded into and run on 7.5% and 10% SDS-Polyacrylamide gel and then electro-blotted onto a nitrocellulose membrane (BioRad Co., Hercules, CA, USA). Transfer of proteins was checked by Ponceau Reagent (0.5% Ponceau S (Sigma), 1% glacial acetic acid (Sigma) in dH$_2$O). Membranes were blocked for 60 min. with 5% non-fat milk in TBS-T (0.1% Tween-20 (Sigma) in 1$\times$ TBS (0.1 M NaCl, 0.1 M Tris pH 7.4 in ddH$_2$O) (All purchased from Numi, National University of Singapore) or 5% Bovine Serum Albumin (BSA, Amresco, Salem, OH, USA) in 1$\times$ TBS-T, depending on the protein probed for. Subsequently, membranes were probed with primary antibodies against target proteins overnight at 4°C. Mouse monoclonal antibodies used were phosphorylated p53 (Ser 15) (p-p53) (Cell Signaling; 1:1000) and p53 DO-1 (Santa Cruz, Santa Cruz, CA, USA; 1:500) and actin (Chemicon, USA; 1:5000). Rabbit polyclonal antibody used was XPB (Santa Cruz; 1:100). The membrane was then incubated in goat anti-mouse IgG (H+L)-HRP (Pierce; 1:5000) or sheep anti-rabbit IgG (H+L)-HRP (Pierce; 1:5000) secondary antibody for 1 hr at room temperature. The protein bands were visualized after incubation of membranes in Chemiluminescence Reagent Plus (Perkin Elmer Life Science Inc., Waltham, MA, USA) followed by exposure to X-ray film (Pierce).

Statistical analysis

Statistical significance between and among data sets was assessed using two-way ANOVA, using Graphpad Prism (Graphpad, La Jolla, CA, USA). The difference was considered to be statistically significant when $P < 0.05$.

Results

XPB$^{-/-}$ cells are less sensitive to the cytotoxic effects of oxidative stress

All three cell types exhibited a common trend of dose dependant decrease in cell viability (Fig. 1). The normal cells appeared to be more sensitive to H_2O_2 induced stress with significantly lower
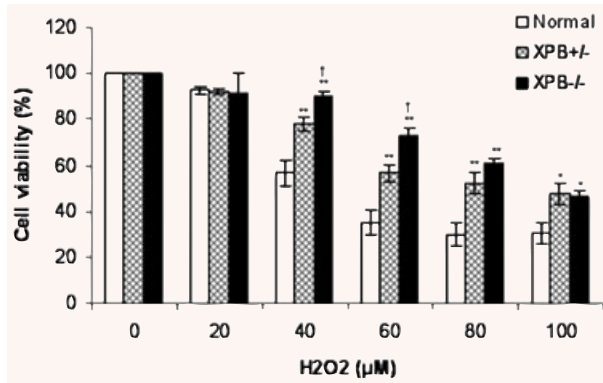
Fig. 1 Dose-dependent decrease in cell viability in H_2O_2 treated cells. $XPB^{-/-}$ and $XPB^{+/-}$ cells are significantly less sensitive to cell death compared to normal cells at concentrations above 20 μM. $*P < 0.05$; $**P < 0.01$ (two-way ANOVA). Data are represented as mean $\pm$ S.E. $XPB^{-/-}$ cells are also significantly less sensitive to cell death compared to $XPB^{+/-}$ cells at 40 μM and 60 μM ($\dagger P < 0.05$).

viability compared to the other two cells types from concentrations of 40 μM and above ($P < 0.05$). $XPB^{-/-}$ cells appeared to be the least sensitive cell type with $XPB^{+/-}$ exhibiting intermediate sensitivity. Interestingly, there was a levelling off of viability decline in normal and $XPB^{+/-}$ cells but not in $XPB^{-/-}$ cells. The differences in the viability trends prompted our investigation of cell cycle changes in the cells following exposure to H_2O_2.

Dysfunctional XPB causes deficiency in cell cycle checkpoint function

Figure 2 A illustrates the cell cycle profiles of normal, $XPB^{+/-}$ and $XPB^{-/-}$ cells after 24 hrs of exposure to H_2O_2. Normal cells displayed a dose dependent shift in cell cycle profiles (Fig. 2B). There was an increase in G2/M phase of cells after 20 μM and 40 μM H_2O_2 in normal cells with a corresponding decrease in G_1 and S phases. Above 40 μM, the G1 and Sub-G_1 populations were greatly increased. $XPB^{+/-}$ cells displayed a similar increase in G2/M followed by G1 populations in $XPB^{+/-}$ cells at the same doses as in normal cells, however there no change in the Sub-G1 population (Fig. 2C). $XPB^{-/-}$ cells presented a little change in profiles up to 40 μM and above this concentration, there was a slight decrease in the G_2/M population with concomitant increases in the G_1 and Sub-G_1 populations (Fig. 2D). To determine if cell cycle profile changes in the cells or lack thereof were associated with DNA damage, we employed the alkaline single cell electrophoresis or comet Assay.

XPB deficient cells show compromised repair capacity for oxidative DNA lesions

A pair of single cell gel electrophoresis (comet) assays was done to determine initial DNA damage at 2 hrs following H_2O_2 exposure

and persisting DNA damage after a 22-hr recovery period. Nuclei with undamaged DNA appear round; nuclei with damaged DNA in the form of strand breaks result in DNA fragments which migrate faster during gel electrophoresis and give rise to a 'tail'. The percentage of DNA in these 'tails' (% tail DNA) was used as a measure of DNA damage.

At 2 hrs, normal cells displayed significant dose dependent increases ($P < 0.001$) in % tail DNA at concentrations from 40 μM. $XPB^{-/-}$ and $XPB^{+/-}$ cells displayed a similar trend from 20 μM ($P < 0.05$). Normal cells displayed significantly lower ($P < 0.001$)% tail DNA compared to the other two cell types ($P < 0.01$) (Fig. 3).

Following the recovery period, there were significant reductions ($P < 0.001$) in % tail DNA for all conditions under which there was damage at 2 hrs (Fig. 3). This returned back toward the baseline is indicative of damage repair. In normal cells there was no significant difference between treated at all concentrations and untreated cells ($P > 0.05$). Treated $XPB^{+/-}$ cells displayed significant differences from untreated cells only from 80 μM ($P < 0.001$). $XPB^{-/-}$ cells exposed to H_2O_2 retained significantly higher ($P < 0.001$)% tail DNA than untreated cells at all doses. Between cell types, $XPB^{-/-}$ cells displayed significantly higher% tail DNA recovery as compared to normal ($P < 0.05$; 20 to 100 μM) and $XPB^{+/-}$ cells ($P < 0.01$; 40 to 100 μM). There was no such significant difference ($P > 0.05$) between recovered normal and $XPB^{+/-}$ cells apart from at 80 μM ($P < 0.01$).

Lack of functional XPB increases incidence of oxidative-stress induced genomic instability

Genomic instability markers were used to assess if loss of XPB function renders cells more susceptible to H_2O_2-induced genomic instability. Micronuclei which are the result of lagging chromosomes and acentric chromosomes being excluded from daughter nuclei following cytokinesis are markers of genome instability. Utilising cytochalasin B, an actin polymerization inhibitor, we arrested cells that completed a single nuclear division at cytokinesis. The numbers and distribution of micronuclei in the resulting binucleates were scored to determine genome stability following exposure to H_2O_2 (Fig. 4). We reduced the H_2O_2 dose range to a maximum of 40 μM as higher concentrations yielded very few mitotic cells and binucleated cells. In congruence to the ability of H_2O_2 to induce DNA strand breaks, all three cell types displayed significant increases in micronuclei frequency following exposure. $XPB^{-/-}$ cells showed significantly higher micronuclei frequency than normal cells when exposed to H_2O_2 ($P < 0.05$). There was no significant difference between $XPB^{+/-}$ and normal cells or between $XPB^{+/-}$ and $XPB^{-/-}$ cells ($P > 0.05$).

Similar to the micronucleus results, all three cell types displayed an increase in chromosomal aberrations in the form of breaks following H_2O_2-induced oxidative stress (Fig. 4B). Importantly, although there were not any significant difference between $XPB^{+/-}$ and normal cells with or without treatment, H_2O_2 proved to be more clastogenic on $XPB^{-/-}$ cells. Following H_2O_2
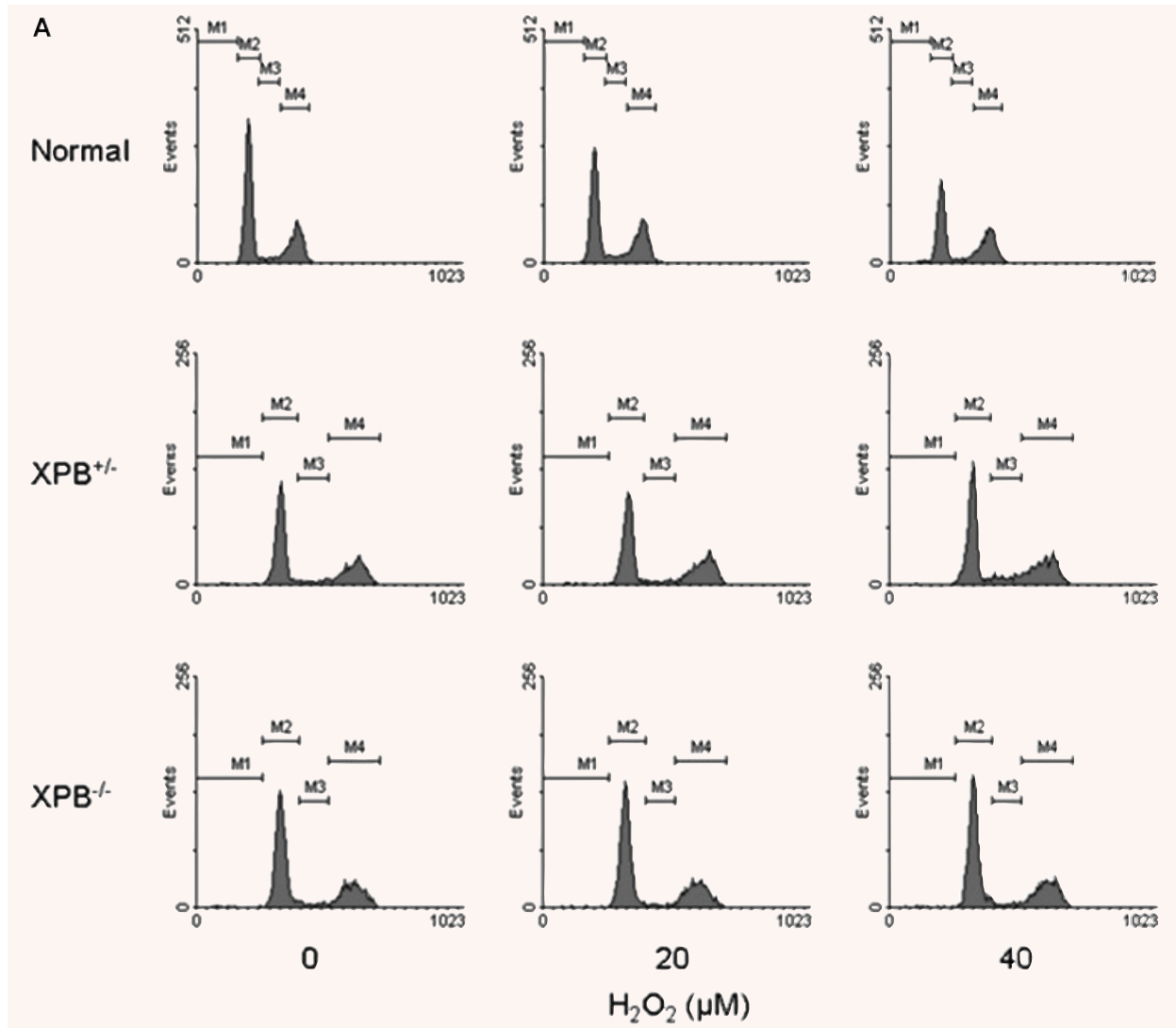
Fig. 2 Cell cycle analysis by FACS. (**A**) Cell cycle histograms 24 hrs after exposure to H_2O_2. Clear profile changes and phase shifts observed in normal and $XPB^{+/-}$ cells. Changes in $XPB^{-/-}$ cells not easily discriminated. (**B**)–(**C**). Percentages of cells in each phase of the cell cycle. (**B**) H_2O_2 affects a G2/M increase at 20 to 40 μM with increases in G1 and sub-G1 populations at subsequent concentrations. (**C**) Similar increase in G2/M followed by G_1 populations in $XPB^{+/-}$ cells at the same doses as in normal cells. Minimal sub-G_1 population observed. (**D**) $XPB^{-/-}$ cells no not display the G2/M increase observed for the latter two cells at 20 to 40 μM. G_1 and sub-G_1 populations increase slightly at subsequent concentrations.

treatment, $XPB^{-/-}$ cells exhibited significantly ($P < 0.05$) higher chromosome aberrations than normal cells.

XPB deficient cells display early appearance of senescent characteristics

Based on the results of the crystal violet assays and cell cycle profiles, we selected a dose of 20 μM to utilize for low dose chronic oxidative stress exposure. This dose caused only slight non-significant decrease in cell viability in all three cell types and did not greatly perturb cell cycle profiles. We also included a set of cells cultured under hyperoxia (40% O_2) for a broader perspective of chronic oxidative stress.

Senescent characteristics included enlarged and flattened cell morphologies, increased cell volume, expression of SA-β-gal and reduced population doubling rate. In the absence of oxidative stress, the enlarged morphologies in $XPB^{-/-}$ cells appeared at day 23 of treatment compared to normal fibroblast morphologies
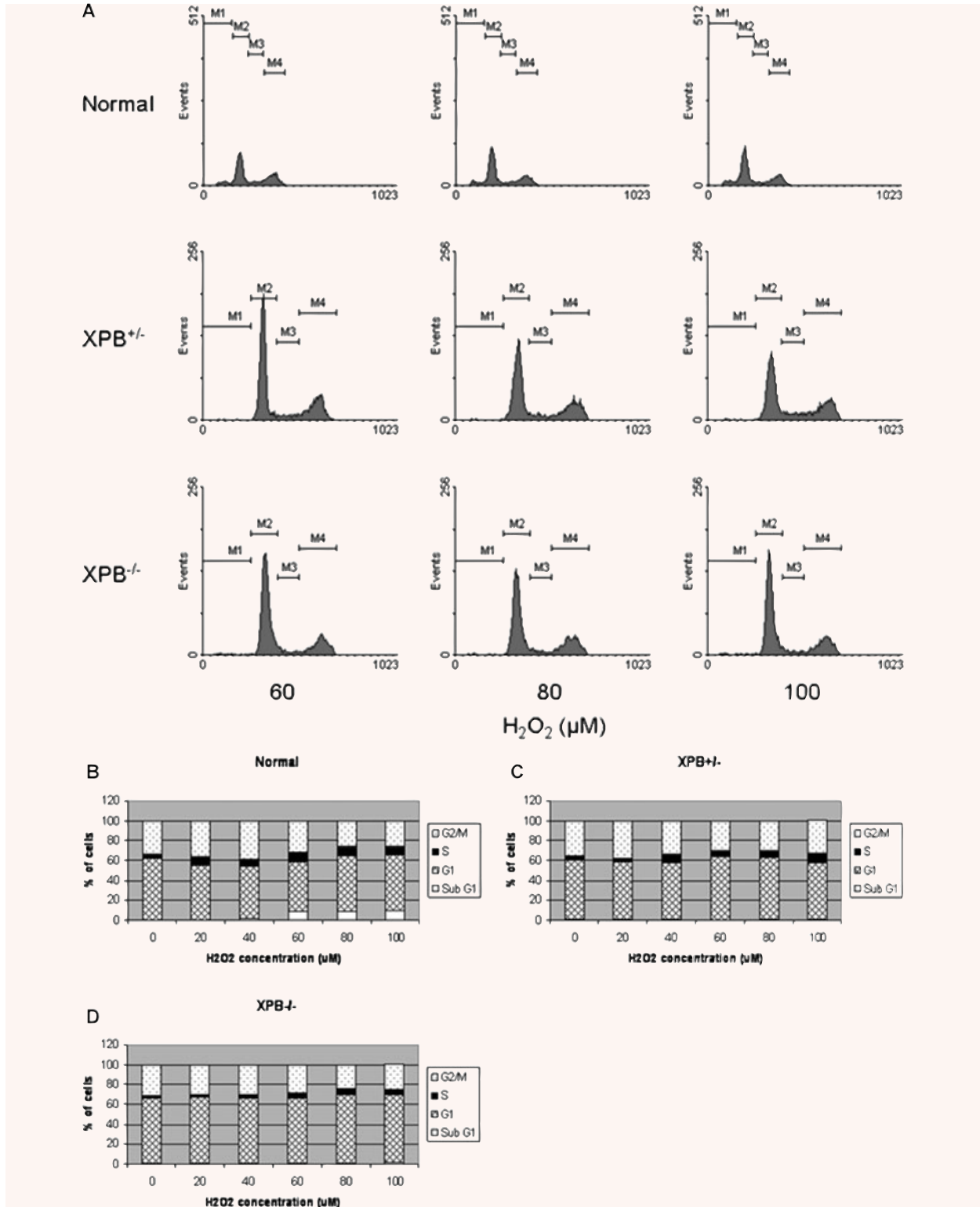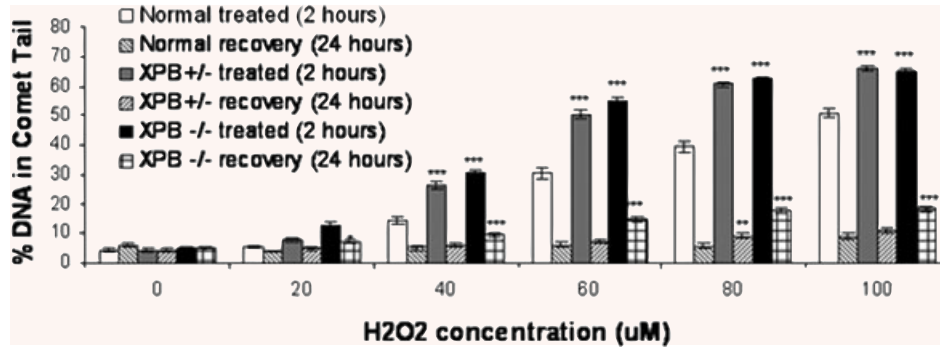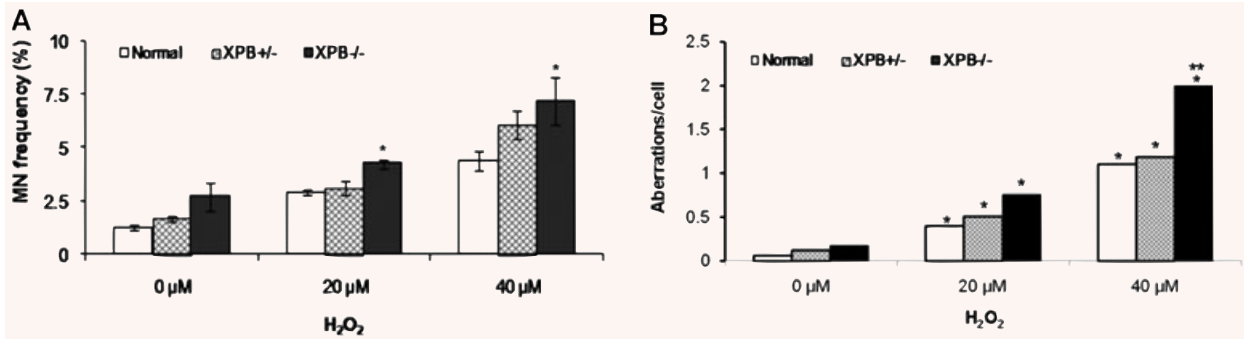
Fig. 2 Continued

Fig. 4 (**A**) Cytokinesis blocked micronucleus assay. Percent MN per 1000 BN scored following H_2O_2 treatment. There was no significant difference between XPB$^{+/-}$ and normal cells ($P >$ 0.05). XPB$^{-/-}$ cells exhibit significantly more MN presence in BN cells compared to control cells. *$P <$ 0.05 (two-way ANOVA). Data are represented as mean ± S.E. (**B**) Chromosome analysis by PNA-FISH: Chromosome analysis was done in metaphase spreads following H_2O_2 treatment. All three cell types displayed an increase in chromosomal aberrations in the form of breaks following H_2O_2-induced oxidative stress (see results for explanation). Chromosome aberrations per cell are displayed for each sample. Chromosome aberrations detected include fragments and breaks. *$P <$ 0.05 compared to untreated sample of respective cell type. **$P <$ 0.05 – Compared to normal and XPB$^{+/-}$ cells after 40 μM H_2O_2 treatment.

throughout the entire period in normal cells (Fig. 5A, B). SA-β-gal expression in XPB$^{-/-}$ was detected at day 24 compared to no expression in normal cells (Fig. 5A, B). XPB$^{+/-}$ cells also displayed typical fibroblastic morphologies and no SA-β-gal expression when not exposed to H_2O_2 or 40% O_2 (Fig. 5A, B).

Exposure to oxidative stress conditions resulted in the appearance of senescent characteristics in normal and XPB$^{+/-}$ cells and hastened their appearance in XPB$^{-/-}$ cells. The latter displayed cell body enlargement as early as day 6 for H_2O_2 and day 11 for 40% oxygen compared to days 9 (H_2O_2) and 17 (40% O_2) for normal cells and days 11 (H_2O_2) and 21 (40% O_2) for XPB$^{+/-}$ cells. SA-β-gal expression in stressed XPB$^{-/-}$ cells

was observed by day 12. Minimal staining was only observed in H_2O_2 treated normal and XPB$^{+/-}$ cells by day 18 and absence of staining with 40% O_2. Interestingly, treatment with H_2O_2 results in earlier appearance of senescent morphologies and positive SA-β-gal staining than 40% O_2. With the latter treatment regime, minimal staining was observed even by the end of the 30-day period. We also observed that XPB$^{+/-}$ cells first manifested senescent morphological changes later than both the other two cell types.

Total population doublings in treated XPB$^{-/-}$ cells were also lower than those in treated normal cells. XPB$^{+/-}$ cells were intermediate in the appearance of these features (Fig. 5C).
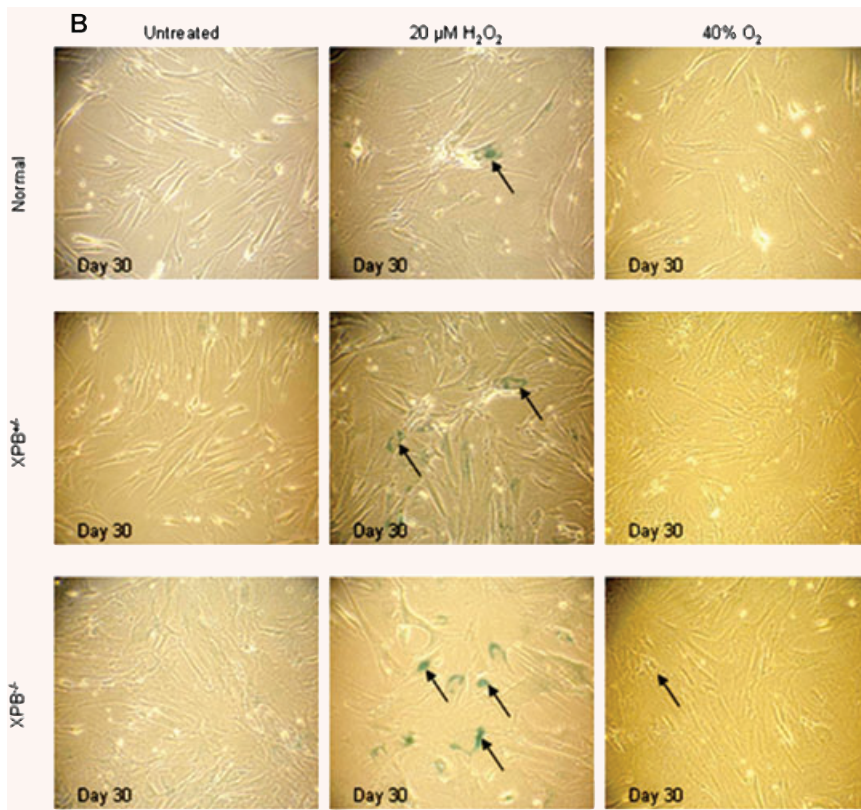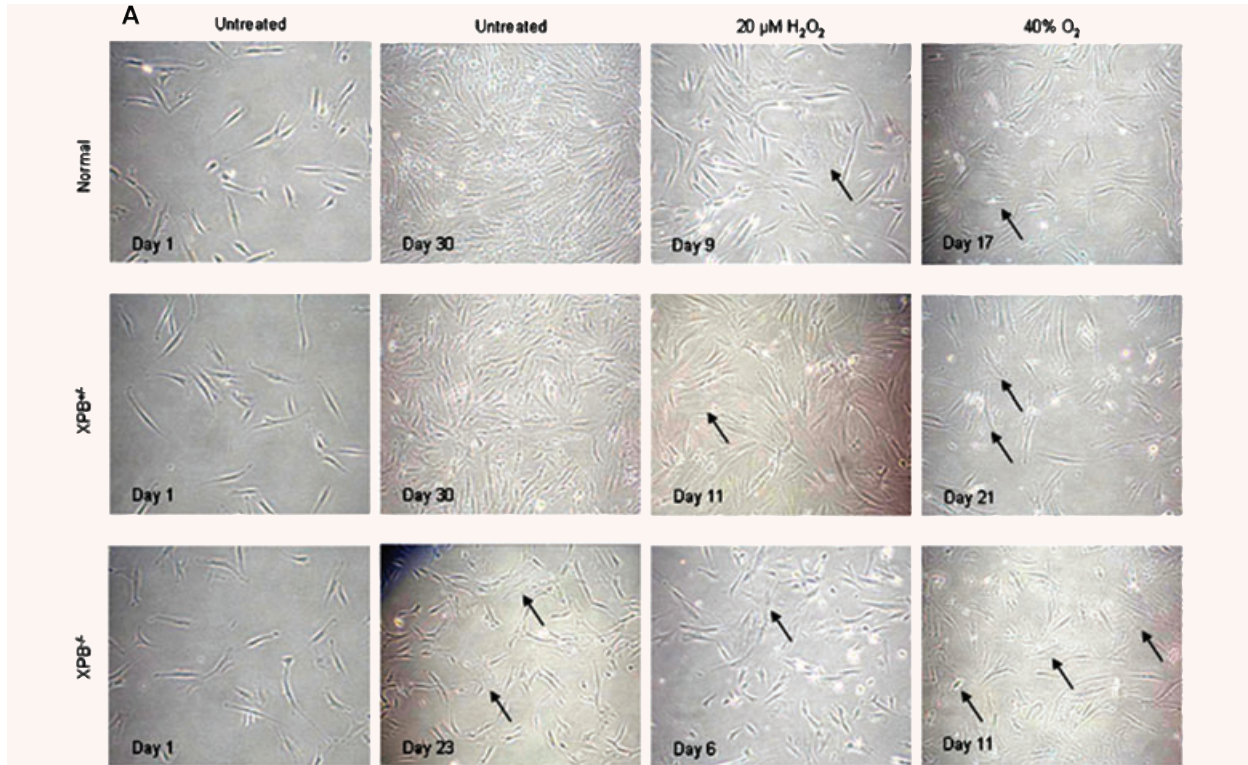
Fig. 5 Cellular kinetics study. (**A**) Morphologies of fibroblasts under chronic oxidative stress at 40× magnification. Typical elongated fibroblast morphology is replaced with enlarged and flattened senescent morphology (arrows) over time and with oxidative stress. Pictures show cells at the start of treatment, on the first day of morphology change. Where no change occurs before the final day, pictures from day 30 are shown. Morphology change takes place earlier in XPB$^{-/-}$ than in the other two cell types in all conditions and hastened by oxidative stress. (**B**) SA-β-gal expression at 100× magnification. Pictures show cells at the end of treatment. Higher incidence of positive staining (bluish; arrows) is present XPB$^{-/-}$ cells than for the other two cell types in all conditions and hastened with oxidative stress. XPB$^{-/-}$ cells also developed blue staining earlier in the treatment period (data not shown) (**C**) Total population doublings undergone by cultures on indicated days throughout the 30-day treatment period. Treated cells displayed reduced total population doublings compared to untreated cells. Treated XPB$^{-/-}$ cells possessed the lowest total population doublings out of all three cell types throughout the investigation.
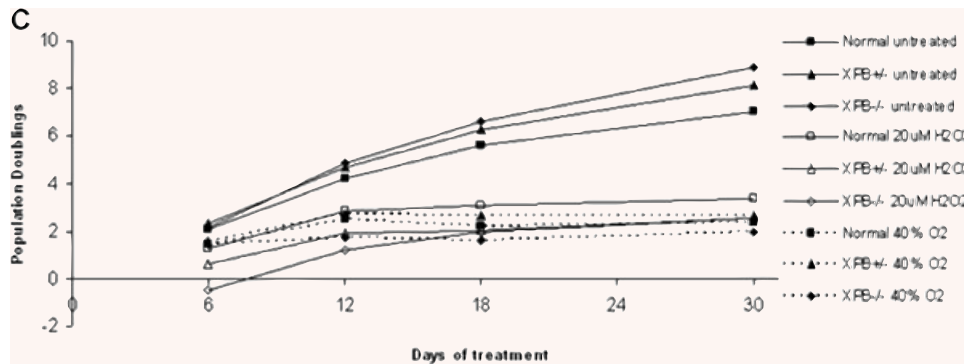
C

Cells lacking XPB exhibit higher telomere attrition

All cells under untreated conditions and exposure to H_2O_2 and 40% O_2 displayed telomere shortening as revealed by TRF length analysis. The raw decreases in TRF length were greater for $XPB^{-/-}$ and $XPB^{+/-}$ cells than for normal cells (Fig. 6B). After taking into account population doubling numbers for the samples, $XPB^{-/-}$ and $XPB^{+/-}$ cells had substantially greater telomere attrition rates than normal cells under oxidative stress conditions (Fig. 6C).

XPB up-regulation occurs as part of normal cellular response to oxidative stress

In normal cells, up-regulation of XPB is evident at 24 hrs after treatment. p53 phosphorylation increased within 2 hrs and p53 up-regulation was observed at 24 hrs; both levels returned to control levels at 48 hrs (Fig. 7A and C). Phosphorylation and up-regulation of p53 phosphorylation and up-regulation was observed at 2 hrs and persisted till 48 hrs in $XPB^{+/-}$ cells. Similarly, up-regulation of XPB occurred in $XPB^{+/-}$ cells at 2 hrs with return towards control levels at 24 and 48 hrs (Fig. 7B and E). In $XPB^{-/-}$ cells p53 up-regulation was seen at 2 hrs with a return to control levels by 48 hrs. XPB up-regulation and a profound increase in p53 phosphorylation were observed at 48 hrs (Fig. 7C and F).

Discussion

It is known that the NER pathway has a function in the repair of DNA lesions induced by oxidative stress. Our data show that $XPB^{-/-}$ cells are resistant to viability decline than normal cells. The ability of $XPB^{-/-}$ to survive in spite of oxidative damage hinted at possible cell cycle checkpoint dysfunction. Obligatory cell cycle arrest occurs when DNA is damaged so as to allow repair or execution of apoptosis if the damage is irreparable. Cell cycle profile shifts upon exposure to genotoxic agents are indications of DNA assault [8, 31]. Lack of cell cycle profile changes in $XPB^{-/-}$ fibroblasts pointed to a cell cycle dysfunction. It was recently reported that XPB has a partially redundant role in p53-mediated apoptotic signalling [32, 33]. Our results of persistence in cell viability and checkpoint dysfunction in $XPB^{-/-}$ fibroblasts are in agreement with these findings. This is significant in light of XPB dysfunction already compromising cell cycle checkpoint response to UV-induced DNA damage [34]; there is now also evidence of checkpoint dysfunction in response to oxidative lesions.

There is an implication that in $XPB^{-/-}$ fibroblasts, the large proportions of cells which have sustained genomic assault and survived also fail to properly repair the damage and can pass this onto progeny. Using alkaline single cell gel electrophoresis or comet assay, we measured tail DNA percentages at two time-points; immediately after the 2-hr exposure period to determine the extent of immediate DNA damage [35] and 22 hrs after removal of H_2O_2 to determine DNA repair or damage recovery [36]. All cells displayed increased tail DNA percentages at the 2-hr mark which subsequently decreased after the recovery period. This is within expectations as all three cell types have a functional base excision repair pathway, the main pathway for alleviating oxidative DNA lesions. Notably, while normal and $XPB^{+/-}$ fibroblasts were able to decrease tail DNA percentages to baseline values, $XPB^{-/-}$ cells retained higher damage after recovery. This is in line with our hypothesis that XPB is involved in proper cellular response to and repair of oxidative lesions. The unrepaired damage in $XPB^{-/-}$ cells could constitute two functional scenarios. The first is that this damage arises from a subset of oxidative lesions that are specifically or preferentially repaired by XPB and its partner factors [13]. However, it was recently reported that a common oxidative DNA adduct, 8-oxoguanine did not require NER factors including XPB for proper excision [37]. The second scenario involves XPB and its partner proteins acting in concert with the BER to expedite repair of oxidative DNA lesions and XPB dysfunction causes a delay in repair. The exhibition of higher tail DNA percentages by $XPB^{+/-}$ and $XPB^{-/-}$ fibroblasts immediately after H_2O_2 exposure is another interesting trend as it is also indicative of a role for XPB in detecting initial oxidative damage, restricting
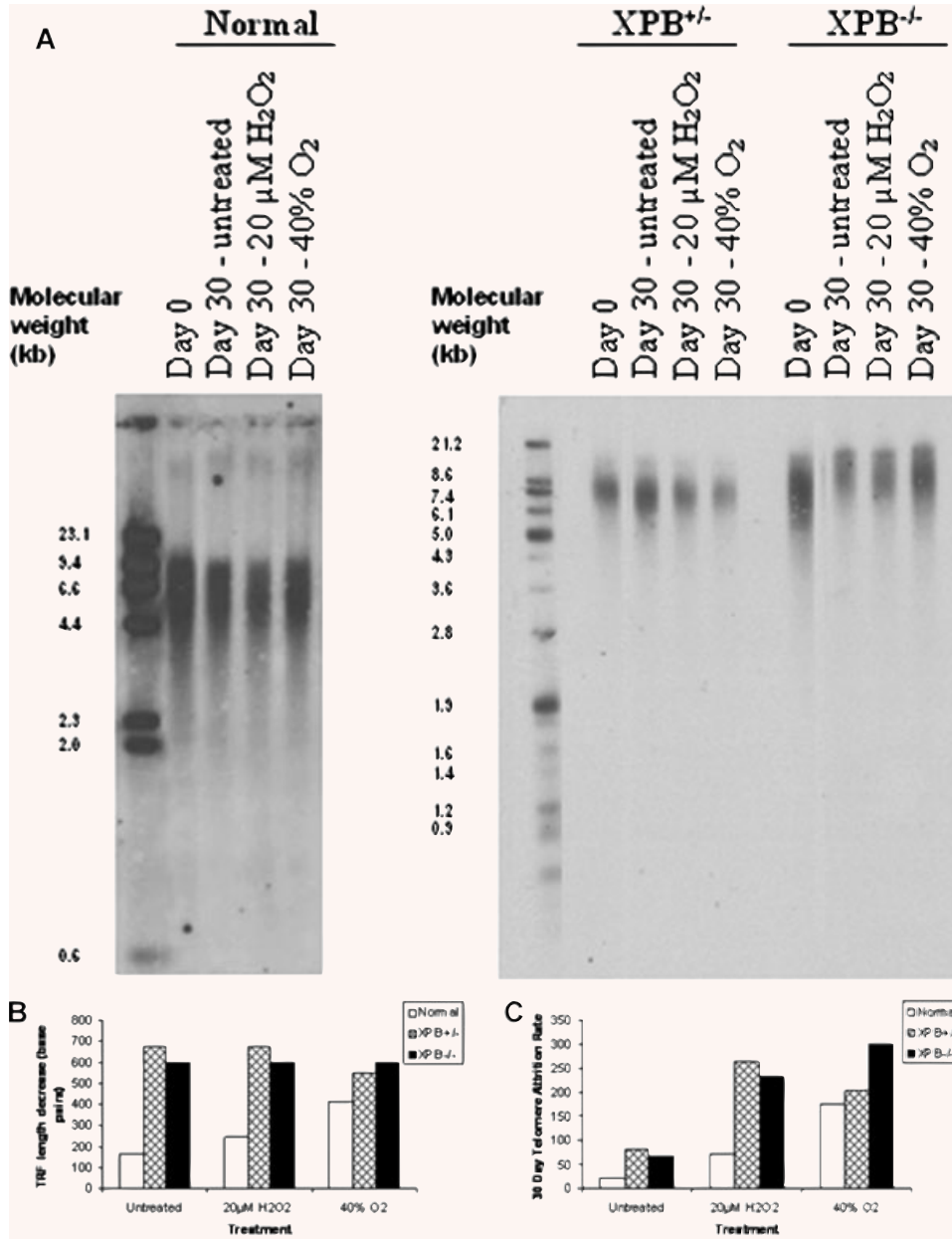
Fig. 6 Telomere restriction fragment analysis (**A**) Southern blot of TRFs obtained by digest of genomic DNA with Hinf1 and Rsal. (**B**) Total TRF length decreases after completion of 30-day period. Both XPB deficient cell types displayed greater decreases of TRF length than normal cells under all conditions. (**C**) Telomere attrition rate derived by dividing the TRF length decrease by the number of population doublings. Attrition rate increases in all cell types under conditions of oxidative stress similar trend to raw TRF length decrease. XPB deficient cell types exhibited a greater attrition rate than normal cells. Attrition rate for XPB$^{-/-}$ was also markedly greater than that for XPB$^{+/-}$ cells at 40% O_2.

its extent or starting the repair process. Support for this phenomenon comes from studies which indicate XPB is important for proper recruitment of other NER factors to UV lesion sites [16] and that the particular mutation (F99S) in our cells reduces opening of DNA surrounding UV-induced lesions [38].

Various syndromes including XP and Ataxia Telangiectasia are caused by DNA repair deficiencies and result in increased disposition to cancers [1, 10, 39–41]. Compromised repair in such cells may result in inheritance of DNA damage by their progeny.

DNA damage such as chromosomal breaks can result in potentially oncogenic changes through the formation of truncated or fusion proteins and misregulation of tumour suppressors and oncogenes [29, 42]. We utilized the micronucleus assay [26, 43] to investigate the presence of accompanying genomic instability. Exposure to oxidative stress induced by H_2O_2 resulted in increased micronuclei frequency which is an expected result as H_2O_2 induces DNA strand breaks. It is notable that this frequency is greater in XPB$^{-/-}$ cells than the other two cell types.
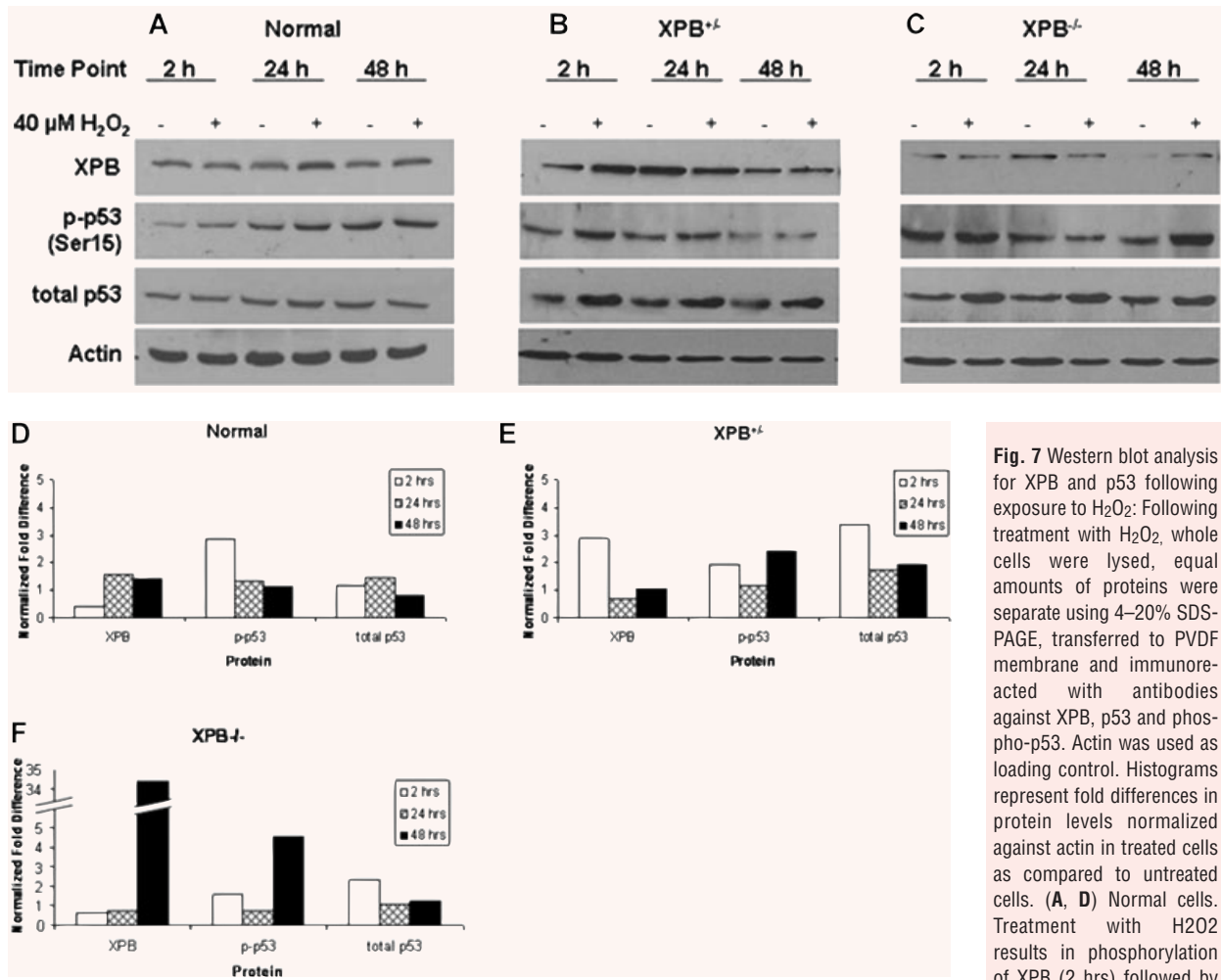
Fig. 7 Western blot analysis for XPB and p53 following exposure to H₂O₂: Following treatment with H₂O₂, whole cells were lysed, equal amounts of proteins were separate using 4–20% SDS-PAGE, transferred to PVDF membrane and immunoreacted with antibodies against XPB, p53 and phospho-p53. Actin was used as loading control. Histograms represent fold differences in protein levels normalized against actin in treated cells as compared to untreated cells. (**A**, **D**) Normal cells. Treatment with H2O2 results in phosphorylation of XPB (2 hrs) followed by up-regulation of XPB and p53 (24 hrs). (**B**, **E**) XPB$^{+/-}$ cells. XPB and p53 up-regulation take place at an earlier time-point (2 hrs) than in normal cells. p53 up-regulation persists till 48 hrs. A lower fold increase in p-p53 than in normal cells was also observed. (**C**, **E**) XPB$^{-/-}$ cells. p53 up-regulation occurs earlier than in normal cells (2 hrs). XPB up-regulation and p53 phosphorylation is delayed till 48 hrs.

Chromosome aberrations detected support this observation. The results from this assay indicate that lack of repair combined with cell cycle checkpoint dysfunction contributes to increased numbers of daughter cells with genomic damage. This agrees with XP-B patients having increased predisposition to developing cancers and implicates oxidative stress as a contributing factor in carcinogenesis in these patients.

It has been widely shown that oxidative stress causes decline in cell viability, cell cycle arrest and DNA damage including enhanced telomere attrition [9, 36]. Induction of oxidative stress affects the proliferative capacity of cells and predisposes premature senescence and ageing. Notably, cells defective in repair

mechanisms such as Ataxia Telangiectasia have been shown to exhibit faster rates of telomere attrition and earlier senescence than normal cells [21, 44]. We performed a group of cellular kinetics studies to address the effects of chronic low level exposure to oxidative stress in relation to XPB. Untreated XPB$^{-/-}$ cells displayed enlarged and flattened cell morphology, SA-β-gal expression and reduced population doubling rates towards the end of the treatment period whereas normal and XPB$^{+/-}$ cells did not. This is significant as it agrees with the segmental progeria presented by XP patients and implicates factors other than UV for this symptom as cell cultures were not exposed to UV sources. Consistent with known findings that H₂O₂ and

hyperoxia induces premature senescence in cells [36, 45], exposure to H_2O_2 and 40% O_2 resulted in morphological changes and SA-β-gal expression in all three cell types. Compared to untreated cells, these changes appeared earliest in XPB$^{-/-}$ cells. We observed that H_2O_2 had a more pronounced effect on all three cell types than 40% O_2. H_2O_2 is only one of a plethora of ROS generated under normal metabolism. Introduction of exogenous H_2O_2 may thus constitute a greater imbalance in cellular redox potential than hyperoxia which in turn gave rise to more pronounced effects. We also found that XPB$^{+/-}$ were almost as adept as normal cells in coping with chronic oxidative stress. The above mentioned partially redundant role of XPB in apoptotic signalling may offer an explanation as one functional copy of the gene is able to compensate along with the other partially redundant factors for the dysfunctional copies.

As well as these morphological changes and marker expression, we observed a heightened telomere attrition rate under oxidative stress, especially when combined with XPB dysfunction. Telomeres cap chromosomal ends and are important for chromosome integrity and segregation [29, 42]. They have been regarded as a determinant in cellular replication, aging and lifespan [2–6]. Telomeres have been shown to preferentially accumulate single stranded regions induced by oxidative stress [46]. Various factors, such as the telomere repeating binding factors TRF1 and TRF2 and telomerase, modulate telomere dynamics and integrity [5]. It has been found that various DNA repair factors function in telomere maintenance and repair of damage sustained at telomeres [19, 47]. These include the helicase domain containing family of proteins [20, 22, 48] of which XPB is a member [20]. As such, the presence of increased telomere attrition in XPB$^{-/-}$ cells is not an unexpected result. Further support comes from studies that show XPF, one of the partner proteins of XPB in the NER pathway is involved in telomere dynamics in mice [23].

The various functional observations made led us to look into the molecular basis behind the previous results. In all cells, XPB was up-regulated following exposure to H_2O_2. Interestingly, up-regulation occurred at divergent time-points in all cells. Up-regulation in XPB$^{+/-}$ cells was present as early as 2 hrs. This might be explained by lower levels of functional XPB in XPB$^{+/-}$ cells compared to normal cells. These cells would thus require an earlier increase in XPB levels following oxidative stress whereas normal cells have a sufficient baseline reservoir allowing for later up-regulation. In XPB$^{-/-}$ cells, up-regulation only occurred at 48 hrs. This is likely due to the very low levels of only dysfunctional protein in these cells. A lag time could arise as other repair factors would be initiated first as the cells attempted to build up sufficient amounts of XPB. We observed both up-regulation and phosphorylation of p53, a cell cycle checkpoint protein and a DNA damage marker, in all three cell types with exposure to H_2O_2. In addition, p53 expression and phosphorylation patterns were different between normal and XPB$^{-/-}$ cells. In normal cells, increased phosphorylation was observed first at 2 hrs with up-regulation following at 24 hrs, with reversion of both to baseline levels at 48 hrs. XPB$^{-/-}$ cells displayed up-regulation at 2 hrs

while phosphorylation was delayed till 48 hrs. XPB$^{+/-}$ cells displayed similar trends to XPB$^{-/-}$ cells. XPB was reported to be able to bind to p53 [49, 50] and have a partially redundant role in p53-mediated apoptotic signalling [32, 33]. Lack of functional XPB in XPB$^{-/-}$ cells might compromise the ability of these cells to properly phosphorylate p53 and trigger DNA damage and possibly apoptotic signalling cascades. This is in agreement with the results of the crystal violet assay showing higher viability in XPB$^{-/-}$ cells following H_2O_2 treatment. The presence of increased p53 phosphorylation in XPB$^{-/-}$ cells at 48 hrs also corroborates the results of the comet assay which indicate compromised recovery and persistence of DNA damage after resolution in normal cells. The earlier increased expression of p53 in these cells might be an attempt to overcome their inability to phosphorylate p53.

In summary, our study has shown that XPB dysfunction sensitizes cells to the genotoxic effects of oxidative stress while reducing the cytotoxic effects. Such a phenomenon can result in genome instability which can predispose cancer and accelerated telomere attrition which may influence aging. This is congruent with XP patients being extremely sensitive to UV-induced skin lesions and cancers. It is however hard for UV-induced DNA damage to explain the full range of XP symptoms. Our findings implicate oxidative stress as a possible major contributor to such manifestations, particularly at tissues away from the body surface and hence protected from UV exposure. This is not surprising given that oxidative stress *via* ROS generation is downstream to a various other genotoxic agents including UV irradiation [8]. It has been shown that polymorphisms in the XPB gene can rise to diseases of varying severities and phenotypes [24, 25]. Additionally, the inclusion of heterozygous cells in our study hint as well at a possible copy number dependence. Our results suggest a role for XPB in the resolution of oxidative stress induced DNA lesions and in telomere dynamics. A recent report suggests that the helicase activity of XPB in NER repair of UV-induced DNA lesions is dispensable while its ATPase activity is essential [38]. Whether this is also true of repair of oxidative lesions and telomere maintenance, and whether these activities are performed exclusively by XPB or in concert with other factors including the rest of the NER and telomere binding proteins is the subject of further research.

Acknowledgements

Conflict of interest statement

The authors have no conflicts of interest to declare.

References

1. **Hoeijmakers JH**. Genome maintenance mechanisms for preventing cancer. *Nature*. 2001; 411: 366–74.
2. **Gilley D, Tanaka H, Herbert BS**. Telomere dysfunction in aging and cancer. *Int J Biochem Cell Biol*. 2005; 37: 1000–13.
3. **Klapper W, Parwaresch R, Krupp G**. Telomere biology in human aging and aging syndromes. *Mech Ageing Dev*. 2001; 122: 695–712.
4. **Levy MZ, Allsopp RC, Futcher AB, *et al***. Telomere end-replication problem and cell aging. *J Mol Biol*. 1992; 225: 951–60.
5. **Rodier F, Kim SH, Nijjar T, *et al***. Cancer and aging: the importance of telomeres in genome maintenance. *Int J Biochem Cell Biol*. 2005; 37: 977–90.
6. **Shay JW, Wright WE.** Telomeres and telomerase: implications for cancer and aging. *Radiat Res*. 2001; 155: 188–93.
7. **Wood RD**. Nucleotide excision repair in mammalian cells. *J Biol Chem*. 1997; 272: 23465–8.
8. **Finkel T, Holbrook NJ**. Oxidants, oxidative stress and the biology of ageing. *Nature*. 2000; 408: 239–47.
9. **von Zglinicki T**. Oxidative stress shortens telomeres. *Trends Biochem Sci*. 2002; 27: 339–44.
10. **Norgauer J, Idzko M, Panther E, *et al***. Xeroderma pigmentosum. *Eur J Dermatol*. 2003; 13: 4–9.
11. **van Steeg H., Kraemer KH**. Xeroderma pigmentosum and the role of UV-induced DNA damage in skin cancer. *Mol Med Today*. 1999; 5: 86–94.
12. **Rybanska I, Pirsel M.** Involvement of the nucleotide excision repair proteins in the removal of oxidative DNA base damage in mammalian cells. *Neoplasma*. 2003; 50: 389–95.
13. **Satoh MS, Jones CJ, Wood RD, *et al***. DNA excision-repair defect of xeroderma pigmentosum prevents removal of a class of oxygen free radical-induced base lesions. *Proc Natl Acad Sci USA*. 1993; 90: 6335–9.
14. **Coin F, Auriol J, Tapias A, *et al***. Phosphorylation of XPB helicase regulates TFIIH nucleotide excision repair activity. *EMBO J*. 2004; 23: 4835–46.
15. **Wakasugi M, Sancar A**. Assembly, subunit composition, and footprint of human DNA repair excision nuclease. *Proc Natl Acad Sci USA* 1998; 95: 6669–74.
16. **Oh KS, Imoto K, Boyle J, *et al***. Influence of XPB helicase on recruitment and redistribution of nucleotide excision repair proteins at sites of UV-induced DNA damage. *DNA Repair*. 2007; 6: 1359–70.
17. **Akoulitchev S, Makela TP, Weinberg RA, *et al***. Requirement for TFIIH kinase activity in transcription by RNA polymerase II. *Nature*. 1995; 377: 557–60.
18. **Lehmann AR**. Nucleotide excision repair and the link with transcription. *Trends Biochem Sci*. 1995; 20: 402–5.
19. **Crabbe L, Jauch A, Naeger CM, *et al***. Telomere dysfunction as a cause of genomic instability in Werner syndrome. *Proc Natl Acad Sci USA*. 2007; 104: 2205–10.
20. **Du X, Shen J, Kugan N, *et al***. Telomere shortening exposes functions for the mouse Werner and Bloom syndrome genes. *Mol Cell Biol*. 2004; 24: 8437–46.
21. **Lee JW, Harrigan J, Opresko PL, *et al***. Pathways and functions of the Werner syndrome protein. *Mech Ageing Dev*. 2005; 126: 79–86.
22. **Opresko PL, Mason PA, Podell ER, *et al***. POT1 stimulates RecQ helicases WRN and BLM to unwind telomeric DNA substrates. *J Biol Chem*. 2005; 280: 32069–80.
23. **Munoz P, Blanco R, Flores JM, *et al***. XPF nuclease-dependent telomere loss and increased DNA damage in mice overexpressing TRF2 result in premature aging and cancer. *Nat Genet*. 2005; 37: 1063–71.
24. **Vermeulen W, Scott RJ, Rodgers S, *et al***. Clinical heterogeneity within xeroderma pigmentosum associated with mutations in the DNA repair and transcription gene ERCC3. *Am J Hum Genet*. 1994; 54: 191–200.
25. **Oh KS, Khan SG, Jaspers NG, *et al***. Phenotypic heterogeneity in the XPB DNA helicase gene (ERCC3): xeroderma pigmentosum without and with Cockayne syndrome. *Hum Mutat*. 2006; 27: 1092–103
26. **Hande MP, Boei JJ, Natarajan AT**. Induction and persistence of cytogenetic damage in mouse splenocytes following whole-body X-irradiation analysed by fluorescence in situ hybridization. II. Micronuclei. *Int J Radiat Biol*. 1996; 70: 375–83.
27. **Hande MP, Boei JJ, Natarajan AT**. Induction and persistence of cytogenetic damage in mouse splenocytes following whole-body X-irradiation analysed by fluorescence in situ hybridization. III.
28. **Newman JP, Banerjee B, Fang W, *et al***. Short dysfunctional telomeres impair the repair of arsenite-induced oxidative damage in mouse cells. *J Cell Physiol*. 2008; 214: 796–809.
29. **Hande MP, Samper E, Lansdorp P, *et al***. Telomere length dynamics and chromosomal instability in cells derived from telomerase null mice. *J Cell Biol*. 1999; 144: 589–601.
30. **Greenwood SK, Hill RB, Sun JT, *et al***. Population doubling: a simple and more accurate estimation of cell growth suppression in the *in vitro* assay for chromosomal aberrations that reduces irrelevant positive results. *Environ Mol Mutagen*. 2004; 43: 36–44.
31. **Barzilai A, Yamamoto K**. DNA damage responses to oxidative stress. *DNA Repair*. 2004; 3: 1109–15.
32. **Spillare EA, Wang XW, von KC, *et al***. Redundancy of DNA helicases in p53-mediated apoptosis. *Oncogene*. 2006; 25: 2119–23.
33. **Bernstein C, Bernstein H, Payne CM, *et al***. DNA repair/pro-apoptotic dual-role proteins in five major DNA repair pathways: fail-safe protection against carcinogenesis. *Mutat Res*. 2002; 511: 145–78.
34. **Marini F, Nardo T, Giannattasio M, *et al***. DNA nucleotide excision repair-dependent signaling to checkpoint activation. *Proc Natl Acad Sci USA*. 2006; 103: 17325–30.
35. **Collins AR**. The comet assay for DNA damage and repair: principles, applications, and limitations. *Mol.Biotechnol*. 2004; 26: 249–61.
36. **Duan J, Duan J, Zhang Z, *et al***. Irreversible cellular senescence induced by prolonged exposure to H2O2 involves DNA-damage-and-repair genes and telomere shortening. *Int J Biochem Cell Biol*. 2005; 37: 1407–20.
37. **Pu YS, Jan KY, Wang TC, *et al***. 8-Oxoguanine DNA glycosylase and MutY homolog are involved in the incision of arsenite-induced DNA adducts. *Toxicol Sci*. 2007; 95: 376–82.
38. **Coin F, Oksenych V, Egly JM**. Distinct roles for the XPB/p52 and XPD/p44 subcomplexes of TFIIH in damaged DNA opening during nucleotide excision repair. *Mol Cell*. 2007; 26: 245–56.
39. **McKinnon PJ.** ATM and ataxia telangiectasia. *EMBO Rep*. 2004; 5: 772–6.

Chromosome malsegregation/aneuploidy. *Mutagenesis*. 1997; 12: 125–31.

40. **Orren DK**. Werner syndrome: molecular insights into the relationships between defective DNA metabolism, genomic instability, cancer and aging. *Front Biosci*. 2006; 11: 2657–71.

41. **mor-Gueret M**. Bloom syndrome, genomic instability and cancer: the SOS-like hypothesis. *Cancer Lett*. 2006; 236: 1–12.

42. **Slijepcevic P, Hande MP, Bouffler SD, et al**. Telomere length, chromatin structure and chromosome fusigenic potential. *Chromosoma*. 1997; 106: 413–21.

43. **Fenech M**. The *in vitro* micronucleus technique. *Mutat Res*. 2000; 455: 81–95.

44. **Tchirkov A, Lansdorp PM**. Role of oxidative stress in telomere shortening in cultured fibroblasts from normal individuals and patients with ataxia-telangiectasia. *Hum Mol Genet*. 2003; 12: 227–32.

45. **Chen Q, Ames BN**. Senescence-like growth arrest induced by hydrogen peroxide in human diploid fibroblast F65 cells. *Proc Natl Acad Sci USA*. 1994; 91: 4130–4.

46. **Petersen S, Saretzki G, von Zglinicki T**. Preferential accumulation of single-stranded regions in telomeres of human fibroblasts. *Exp Cell Res*. 1998; 239: 152–60.

47. **Hande MP**. DNA repair factors and telomere-chromosome integrity in mammalian cells. *Cytogenet Genome Res*. 2004; 104: 116–122.

48. **Crabbe L, Verdun RE, Haggblom CI, et al**. Defective telomere lagging strand synthesis in cells lacking WRN helicase activity. *Science*. 2004; 306: 1951–3.

49. **Leveillard T, Andera L, Bissonnette N, et al**. Functional interactions between p53 and the TFIIH complex are affected by tumour-associated mutations. *EMBO J*. 1996; 15: 1615–24.

50. **Wang XW, Yeh H, Schaeffer L, et al**. p53 modulation of TFIIH-associated nucleotide excision repair activity. *Nat Genet*. 1995; 10: 188–95.